Organic & Biomolecular Chemistry

www.rsc.org/obc

Volume 7 | Number 19 | 7 October 2009 | Pages 3881–4132

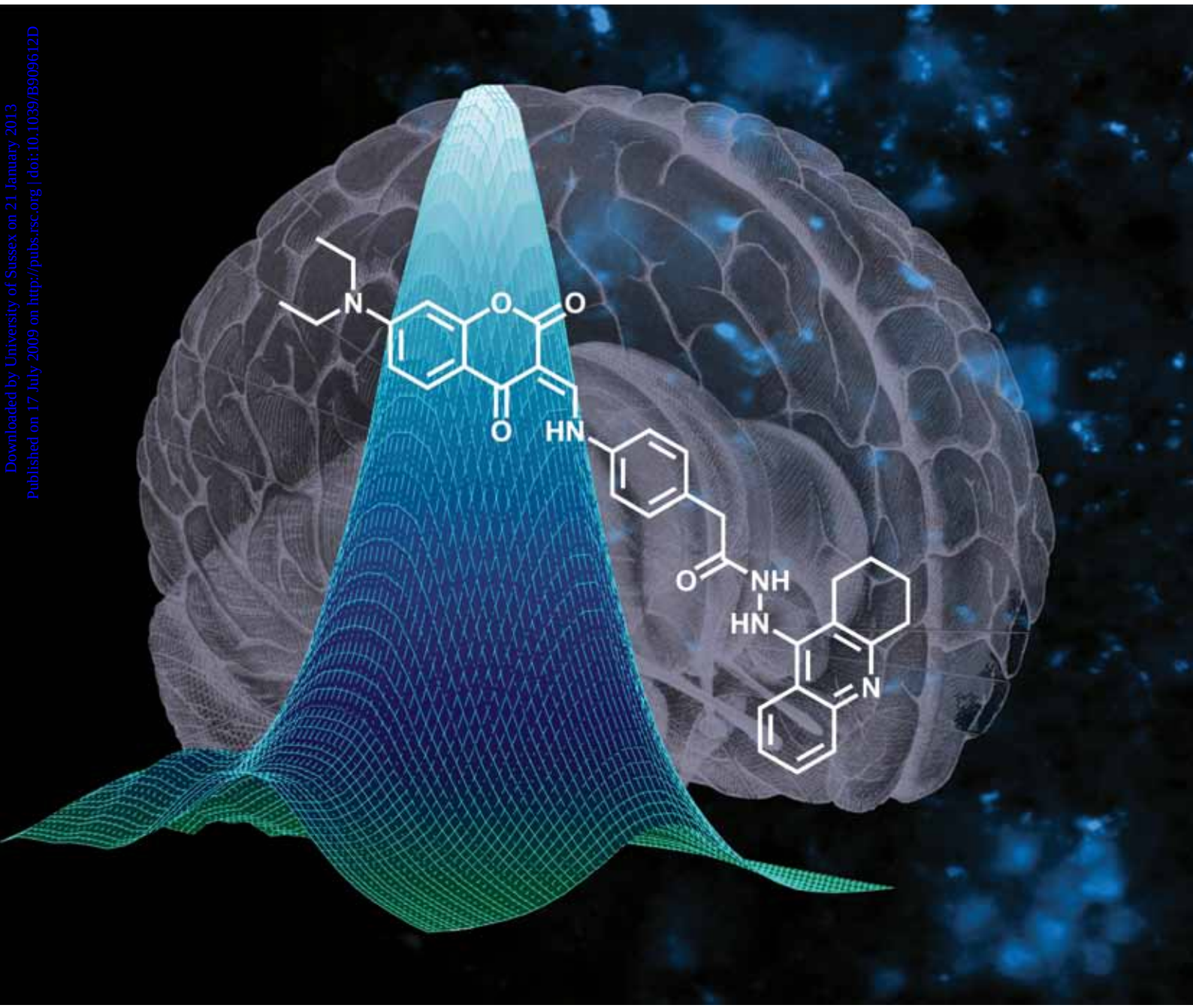

ISSN 1477-0520

FULL PAPER
Paul W. Elsinghorst *et al.*
A gorge-spanning, high-affinity cholinesterase inhibitor to explore β-amyloid plaques

EMERGING AREA
Roger D. Rasberry and Ken D. Shimizu
Molecular playdough: conformationally programmable molecular receptors based on restricted rotation

RSC Publishing

A gorge-spanning, high-affinity cholinesterase inhibitor to explore β-amyloid plaques†

Paul W. Elsinghorst,[a] Wolfgang Härtig,[b] Simone Goldhammer,[b] Jens Grosche[b,c] and Michael Gütschow*[a]

Received 14th May 2009, Accepted 16th June 2009
First published as an Advance Article on the web 17th July 2009
DOI: 10.1039/b909612d

Cholinesterases are involved in the pathological formation of β-amyloid plaques. To investigate this pathohistological hallmark of Alzheimer's disease we prepared a high-affinity, fluorescent cholinesterase inhibitor. Its fluorescence intensity was significantly enhanced upon binding to cholinesterases. Using this probe, brain samples from mice and humans affected by Alzheimer's disease were successfully analyzed for β-amyloid plaques. Unexpectedly, it was discovered, by competition experiments, that the compound binds to amyloid structures, rather than to cholinesterases inside of the plaques.

Introduction

Degeneration of cholinergic neurons in the brain of Alzheimer patients has led to the cholinergic hypothesis as an attempt to describe the pathogenesis of Alzheimer's disease (AD). Accordingly, first symptomatic treatment of AD was realized by inhibiting the acetylcholine-degrading enzymes, mainly acetylcholinesterase (AChE).[1] The active site of AChE and butyrylcholinesterase (BChE) is located at the end of a gorge reaching deep into the protein. Substrates and ligands are guided into and through the gorge by a negative surface charge.[2] The peripheral anionic site (PAS) of AChE is characterized by a highly conserved tryptophan that is commonly found cation–π or π–π interacting with aromatic ligand moieties. An aromatic π–π stacking at the PAS is a feature often utilized by bifunctional inhibitors simultaneously targeting both the active and peripheral binding site.[3]

Senile plaques composed of hardly soluble β-amyloid (Aβ) peptides and neurofibrillary tangles consisting of hyperphosphorylated, microtubule-associated protein τ are known histopathological hallmarks of AD. The formation of β-amyloid by either α- or β-secretase, followed by γ-secretase (presenilin-1) leads to either non-amyloidogenic p3 or to Aβ, which might—in pathologically elevated concentration—accumulate in β-amyloid plaques.[4]

Silver stains, according to Bielschowsky, Gallyas or Braak, are staining methods indicating both main hallmarks of AD.[5] Congo red and thioflavins selectively target the β-sheet structures in senile plaques.[6] Once staining techniques recognizing cholinesterase activity had been developed,[7,8] the deposition of AChE in plaques became evident. Further improvements of these methods led to qualitative and semi-quantitative activity estimates of both AChE and BChE inside β-amyloid plaques.[9,10] Recently developed immuno-(histochemical) techniques allow for the sensitive detection of both β-amyloid plaques and the co-localized AChE.[6]

Further investigations of the AChE and BChE activity originating from β-amyloid plaques revealed, that the inhibition characteristics of cholinesterases located inside β-amyloid plaques differ notably from those in unaffected tissue.[11,12] While it was shown that Aβ itself does not possess cholinesterase activity,[13] it remains to be elucidated how the cholinesterase activity is changed. Thus, it would be worthwhile to establish a probe, that could reflect functional changes of β-amyloid-associated AChE. Valuable fluorescent probes, either gorge-spanning[14,15] or single-binding-site directed[16,17] irreversible inhibitors, have been developed. A competitive inhibitor with gorge-spanning properties addressing both binding sites in native constitution could be useful to characterize AChE inside β-amyloid plaques (Chart 1). We envisaged a fluorescent probe originating from previously established heterodimeric cholinesterase inhibitors.[18,19] The novel probe was designed as a non-irreversible, mixed-type inhibitor with a fluorophore located at the PAS, while a linker would span the gorge to place a tacrine-derived moiety at the active site. Tissues from an AD case and triple-transgenic mice with age-dependent β-amyloidosis and τ-hyperphosphorylation were used to reveal its histological properties.[20]

Results

Synthesis

In accordance with previous reports that revealed the coumarin ring system as a promising moiety of ligands for both AChE[21] and Aβ,[22] the fluorogenic moiety was derived from the 7-aminocoumarin skeleton. In particular, its planar electron-rich aromatic system was anticipated as a versatile interaction partner for Trp286,[3] which plays the fundamental role in PAS binding. As depicted in Scheme 1, malonic acid (**2**) was converted to the activated bis(2,4,6-trichlorophenyl) ester **3** since alkyl esters turned out to be too unreactive for the following reaction step. Compound **3** was subsequently condensed with 3-diethylaminophenol (**4**), in

[a]*Pharmaceutical Institute, Pharmaceutical Chemistry I, University of Bonn, An der Immenburg 4, D-53121, Bonn, Germany. E-mail: guetschow@uni-bonn.de; Fax: +49 228 732567; Tel: +49 228 732317*
[b]*Paul Flechsig Institute for Brain Research, Department for Neurophysiology, University of Leipzig, Jahnallee 59, D-04109, Leipzig, Germany*
[c]*Interdisciplinary Center of Clinical Research (IZKF), Faculty of Medicine, University of Leipzig, Inselstraße 22, D-04103, Leipzig, Germany*

† Electronic supplementary information (ESI) available: Syntheses and elemental analyses of compounds **3**, **5**, **8**, and **10–12**, Lineweaver–Burk analysis, fluorescence experiments, labeling of senile plaques with **13** in the presence and absence of fasciculin-2, histochemical enzyme activity assay with different concentrations of **13**, NMR spectra of compounds **3**, **5**, **8**, and **10–13**, and mass spectrometry analysis of **13**. See DOI: 10.1039/b909612d

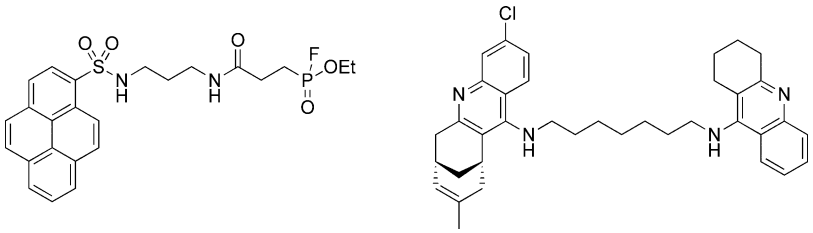

Chart 1 Examples of gorge-spanning, linker-connected cholinesterase inhibitors: a pyrene-labelled phosphonofluoridate[14] (left) and a huprine–tacrine heterodimer[3] (right). Our design combines a fluorophore and tacrine *via* a spacer of similar length.

which 7-hydroxyquinolone formation[23] is prevented because of its diethyl substitution, producing the fluorescent 7-diethylamino-4-hydroxycoumarin (**5**).[24] The attachment of the fluorophore was intended to proceed *via* an enamine formation involving 4-aminophenylacetic acid. It was suitable to hold the tacrine moiety by a hydrazide bond, while the methylene group added flexibility to the linker, that would have been missed using the more common 4-aminobenzoic acid. Thus, 4-nitrophenylacetic acid (**9**) was converted to its hydrazide **10** *via* the corresponding ethyl ester and reacted with 9-chloro-1,2,3,4-tetrahydroacridine (**8**), which in turn was obtained by Friedländer condensation of anthranilic acid (**6**) and cyclohexanone (**7**). The reaction joining the tacrine moiety to the hydrazide involved the use of sealed reaction vessels. The resulting nitrophenyl-substituted tacrine derivative **11** was then reduced to **12** using tin(II) chloride dihydrate, as the application of Pd/C or Ra/Ni interfered with the hydrazide bond. Applying a reaction originally developed by Knierzinger and Wolfbeis,[24] the enamine formation between **5** and **12** producing **13** was achieved using triethyl orthoformate in refluxing glacial acetic acid.

Cholinesterase inhibition

Compound **13** was found to be a potent inhibitor of both human acetylcholinesterase (hAChE) and butyrylcholinesterase (hBChE) *in vitro*. Half-maximal inhibitory concentration (IC_{50}) values of 280 ± 10 pM for hAChE and 16 ± 1 nM for hBChE were determined at 500 μM concentration of the corresponding thiocholine ester substrates. Additionally, Lineweaver–Burk analysis of kinetic measurements in the presence of different substrate and inhibitor concentrations was carried out (see S5 of the ESI†). Assuming a mixed-type inhibition mechanism, the dissociation constants K_{ic} and K_{iu} were determined from secondary plots, where K_{ic} (hAChE: 0.21 ± 0.06 nM, hBChE: 3.5 ± 0.1 nM) describes the competitive and K_{iu} (hAChE: 0.25 ± 0.04 nM, hBChE: 14 ± 2 nM) the uncompetitive contribution to binding of **13** to hAChE or hBChE.[18] The resulting value of $\alpha = K_{iu}/K_{ic}$ (hAChE: 1.2 ± 0.4, hBChE: 4.0 ± 0.4) was considered to characterize the interaction of **13** with the active and peripheral binding site. For hAChE, a value close to 1 suggests a similar affinity of **13** for the free enzyme as for the enzyme–substrate complexes, *i.e.* the Michaelis complex and the acetyl-enzyme. Affinity to these enzyme–substrate complexes may arise from interactions between the inhibitor and amino acid residues not involved in substrate binding, *e.g.* the PAS of hAChE. Due to their architectural differences, peripheral binding to hBChE is expected to be less pronounced.[3] This is reflected in the observed value $\alpha > 1$, indicating a higher affinity of **13** for the free enzyme. For both cholinesterases, the competitive inhibition is expected to result from the typical cation–π stacking of the tacrine heterocycle slipping in between the active-site residues Trp86/82 (hAChE/hBChE) and Tyr337 (hAChE) or Ala328 (hBChE). Such a binding mode has been predicted for several heterobivalent tacrine derivatives.[3,25–27]

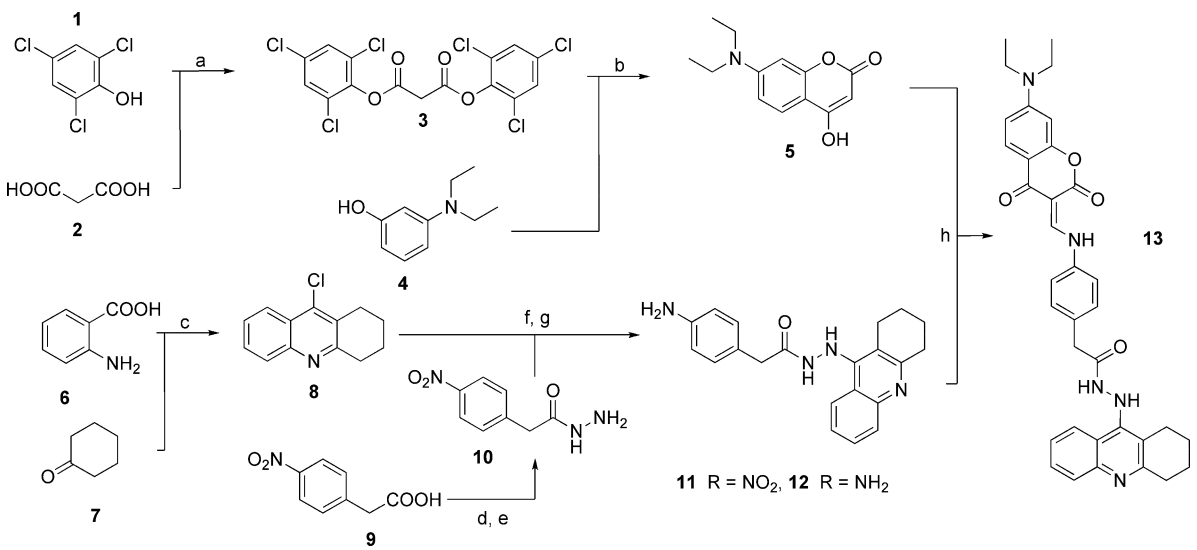

Scheme 1 Synthesis of the fluorescent AChE inhibitor **13**: a) $POCl_3$, reflux, 3 h; b) PhMe, reflux, 2 h; c) $POCl_3$, reflux, 2 h; d) $SOCl_2$, EtOH, RT, 1 h; e) N_2H_4, EtOH/H_2O, 80 °C, 1 h; f) EtOH, 140 °C, 18 h; g) $SnCl_2 \times 2\ H_2O$, EtOH, 70 °C, 2 h; h) $HC(OEt)_3$, AcOH, reflux, 10 min.

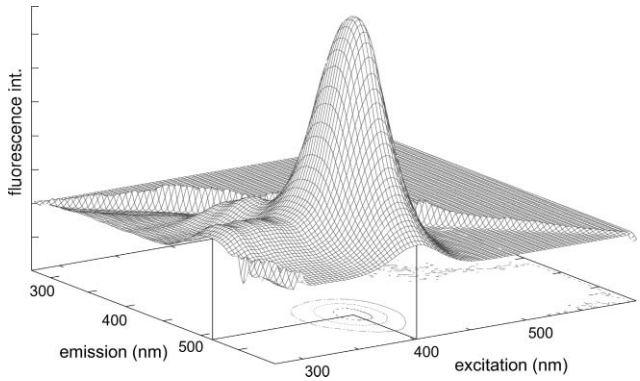

Fig. 1 A 3D fluorescence plot of **13** showing an excitation–emission peak at $\lambda_{exc} = 405$ nm and $\lambda_{em} = 517$ nm.

Fluorescence properties and histochemistry

The fluorescence properties of **13** were investigated by a 3D scan, recording emission spectra from 200–600 nm while excitation was subsequently tuned from 200–600 nm. A surface plot for the 275–600 nm interval revealed an excitation–emission peak with $\lambda_{exc} =$ 405 nm and $\lambda_{em} = 517$ nm (Fig. 1). For subsequent histochemical experiments, this sharp excitation–emission peak in a wavelength range beyond 400 nm was considered very suitable, as only low background due to tissue auto-fluorescence was expected.

In addition, the influence of protein binding on the fluorescence properties of **13** was investigated (Fig. 2, see also S6 of the ESI†). A strong enhancement in fluorescence intensity was observed when **13** was allowed to bind to an excess of hAChE or hBChE in buffered solution. Unspecific binding as a cause of this finding was excluded by control experiments using bovine serum albumin (BSA). In both cases, hAChE and hBChE, an excess of donepezil, a highly potent AChE inhibitor ($IC_{50} = 5.7$ nM),[28] displaced **13** from the gorge, resulting in a loss of fluorescence intensity.

The properties of **13** as a histological dye detecting β-amyloid plaques were revealed by confocal laser scanning microscopy (CLSM). Plaques containing **13** were found in brain tissue sections from triple-transgenic mice (Fig. 3A), carrying, as transgenes, mutated human β-amyloid precursor protein, presenilin-1 and τ, and from an autoptic case with Alzheimer's disease (Fig. 3B). In both tissues, β-amyloid plaques were simultaneously visualized using a rabbit-anti-β-amyloid and red-fluorescent carbocyanine 3-conjugated goat-anti-rabbit IgG (Fig. 3A′ and 3B′). Merged staining patterns clarified the allocation of **13**, color-coded in green, and red-fluorescent β-amyloid-immunoreactivity within the same senile plaques (Fig. 3A″ and 3B″). Both application sequences, either **13** or immunostaining first, were carried out and no difference was observed. Notably, the human tissue showed that **13** has a tendency to highlight the core regions of β-amyloid plaques where AChE may actually be expected to serve as a seed for Aβ aggregation.[29–31] It has been reported that not only the entire enzyme, but also truncated peptides, *e.g.* sequences corresponding to the ω-loop, can act as structural motifs to promote Aβ fibril formation.[29,30,32]

To corroborate our initial conclusion, that **13** binds to AChE inside plaques, staining experiments were subsequently repeated in the presence and absence of fasciculin-2, a peptidic ($M_r = 6500$, $IC_{50} = 24$ nM),[33] high-affinity AChE inhibitor (see S8 of the ESI†). No significant difference in staining by **13** (6.8 μM) was observed as a result of the presence or absence of fasciculin-2 (3.1 μM). A reduction in fluorescence after treatment with fasciculin-2 would have provided ultimate proof of **13** binding to AChE inside β-amyloid plaques. The unaltered observation leads to further questions, *e.g.* whether fasciculin-2 will penetrate into the β-amyloid plaque core, and whether fasciculin-2 can bind to AChE inside the lattice of aggregated Aβ. To exclude molecular size as a question of debate, comparable experiments were carried out using donepezil hydrochloride ($M_r = 416.0$), which occupies the enzyme gorge in a similar fashion as expected for **13**. Again, no attenuation of staining intensity caused by **13** (6.8 μM) was observed in brain samples pretreated with donepezil (145 μM) as shown in Fig. 4. The same result was observed after simultaneous application of equipotent concentrations (145 μM donepezil, 6.8 μM **13**) or excess of donepezil (1450 μM, 6.8 μM **13**).

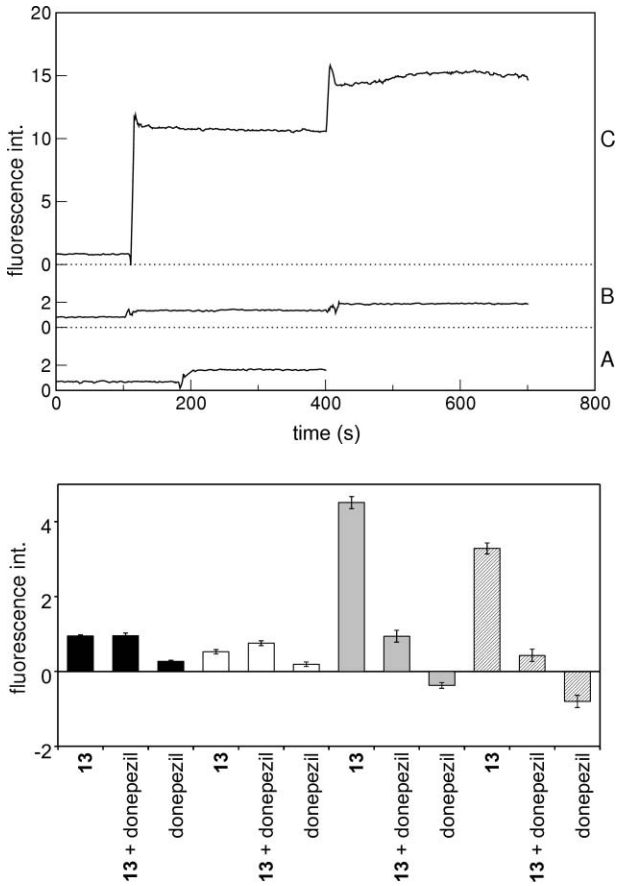

Fig. 2 An increase in fluorescence intensity ($\lambda_{exc} = 405$ nm, $\lambda_{em} = 517$ nm) was observed when **13** (20 nM) was allowed to bind to hAChE (top). Section A shows the fluorescence intensity of **13** added to assay buffer after 200 s. The experiments shown in sections B and C were performed in the presence of 180 nM BSA (B) or hAChE (C). Proteins were added after a blank recording of 100 s, followed by equilibration and addition of **13** after 400 s. The same effect was observed for hBChE (bottom: black = assay buffer, white = BSA, gray = hAChE, hatched = hBChE). Binding of **13** to hAChE or hBChE could be suppressed by 4 μM donepezil (*i.e.* the 10-fold equipotent concentration), where the fluorescence intensity returned to buffer level. A decrease in fluorescence intensity, observed when donepezil was solely applied, can be attributed to impaired auto-fluorescence of both cholinesterases upon donepezil binding.

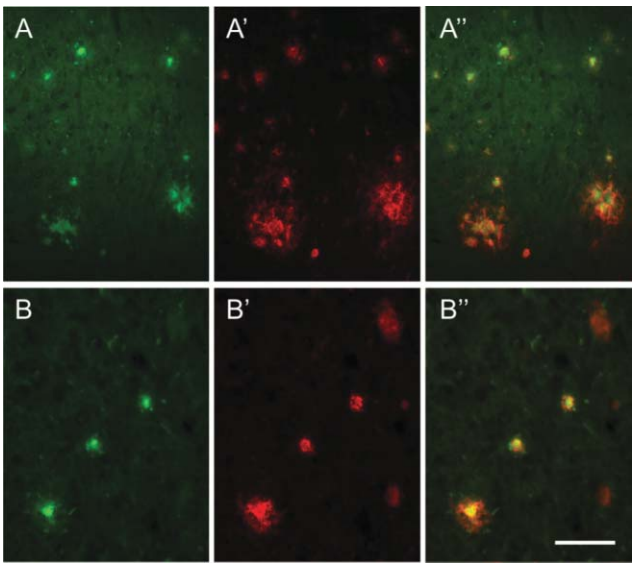

Fig. 3 Double fluorescence labeling of senile plaques with 6.8 μM **13** and β-amyloid-immunoreactivity in the hippocampus of triple-transgenic mice with age-dependent β-amyloidosis (A) and in the area 7 of the neocortex from a case with AD (B). CLSM demonstrates the fluorescence labeling with **13** (A and B), whereas A′ and B′ display indirect immunofluorescence of the same tissue based on rabbit-anti-β-amyloid and red-fluorescent carbocyanine 3-conjugated goat-anti-rabbit IgG. The merged figures A″ and B″ reveal the occurrence of both markers in close vicinity within the same plaques (scale bar = 100 μm).

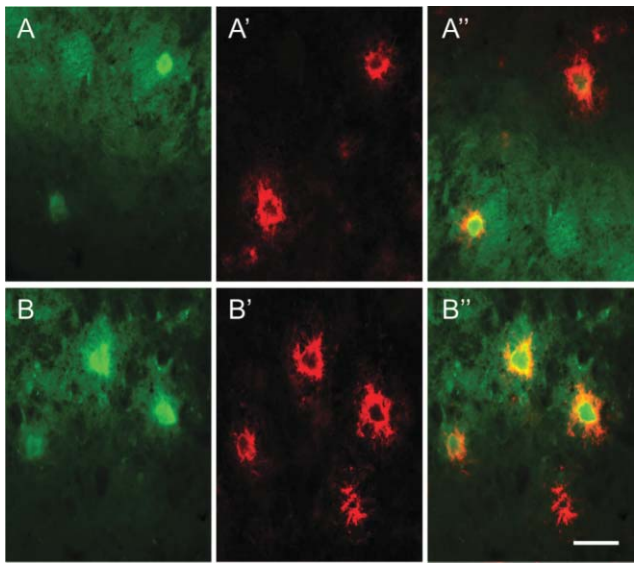

Fig. 4 Double fluorescence labeling of senile plaques in the hippocampus from a 16-month-old triple-transgenic mouse with age-dependent β-amyloidosis. CLSM reveals the combined staining with 6.8 μM **13** (A and B) and Aβ-immunodetection of the same tissue based on rabbit-anti-β-amyloid and red-fluorescent carbocyanine 3-conjugated anti-rabbit IgG (A′ and B′) after pretreatment of tissue sections with 145 μM donepezil (A–A″) or without pretreatment (B–B″). The allocation of both markers in the same plaques becomes obvious in the merged figures A″ and B″ (scale bar = 25 μm).

Binding of **13** to AChE inside β-amyloid plaques seems therefore rather unlikely.

To elucidate whether **13** will bind to tissue-bound AChE at all, we switched from competition experiments to inhibition measurements of tissue-bound AChE by **13**. Tissue sections from brain areas rich in cholinergic neurons were prepared and acetylthiocholine-cleaving AChE activity was investigated. A reduced AChE activity was detected as a decrease in precipitation of dark copper ferrocyanide, that results from the reduction of soluble copper ferricyanide by thiocholine.[34]

A significant inhibition of AChE by **13** was observed in the medial septum-diagonal band complex of the basal forebrain and the hippocampal CA3 region of a triple-transgenic mouse, as well as the apparently identical AChE inhibition by **13** in the cingulate cortices of triple-transgenic and wild-type mice (Fig. 5). Binding of **13** to tissue-bound AChE was further affirmed observing a concentration-dependent inhibition. With increasing

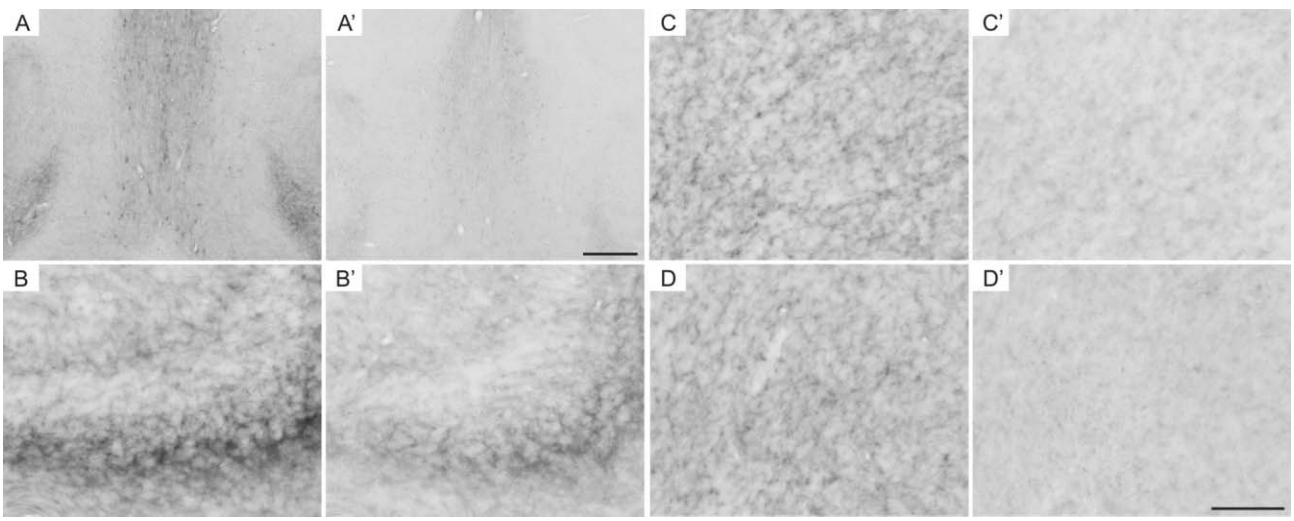

Fig. 5 AChE activity (90 min, 37 °C) histochemically detected without (A–D) and after pretreatment with 68 μM **13** (A′–D′). Medial septum/diagonal band complex of the basal forebrain from a triple-transgenic mouse (A and A′). Hippocampal CA3 region in a triple-transgenic mouse (B and B′). Cingulate cortices in a triple-transgenic mouse (C and C′) and a wild-type mouse (D and D′) (scale bars: A = 300 μm, B–D = 100 μm).

concentrations of **13** (between 68 nM and 68 μM), less AChE activity was detected in the dorsal striatum of a triple-transgenic mouse (see S9 of the ESI†).

Discussion

To establish a probe, that could reflect the interplay between β-amyloid plaques and AChE, we designed a fluorescent, dual-mode inhibitor exploiting the unique enzyme architecture. The inhibitor incorporates two distinct binding moieties, each of them directed either toward the peripheral, or the active site of AChE. A convergent synthesis was devised in which the coumarin fluorophore **5** was combined with the active-site-directed tacrine derivative **12** where phenylacetic acid was chosen to add sufficient flexibility. Moreover, this synthon is of comparable length to the favored 8–9 methylene groups.[18]

Detailed kinetic analysis revealed that **13** is a picomolar inhibitor of hAChE, while being 15-fold less active against hBChE. Furthermore, the dual-binding mode, anticipated from the tailored structure was confirmed as the analysis showed a mixed-type inhibition pattern. An α value of 1.2 ± 0.4 was obtained for hAChE implying virtually equal affinity of **13** for both the free and substrate-bound enzyme.

A strong enhancement in fluorescence intensity of **13** was observed in the presence of the target proteins, hAChE and hBChE, but not BSA. As hBChE lacks a tryptophan at the gorge entrance, interaction of the fluorophore with this residue at the PAS of hAChE cannot satisfactorily explain the effect on both cholinesterases. While the PAS is accessible to water and rather hydrophilic, probably the hydrophobic environment offered by a somewhat deeper part of the gorge accounts for the amplified fluorescence intensity. Alternatively, at least a portion of **13** might be accommodated along the gorge in a reversed manner with the fluorophore orientated to its bottom and the tacrine moiety at the PAS. An additional binding site for tacrine near the PAS has been predicted from investigations with homodimeric tacrine inhibitors.[35]

Donepezil was considered an adequate agent for competition experiments as it is a highly potent inhibitor with molecular weight and physicochemical properties similar to **13**. When bound to AChE, the donepezil molecule spans the entire length of the gorge interacting through aromatic stacking with the anionic subsite at the bottom of the gorge as well as the peripheral site.[3] We have demonstrated that donepezil, in a 10-fold equipotent concentration, does successfully compete with **13** for accommodation within the active-site gorge. These experiments provide additional evidence for the binding mode of **13** within the gorge and, furthermore, support our conclusions from histochemical competition experiments.

Inhibitor **13** proved suitable for histochemical applications and enabled us to examine brain tissues from mice and humans affected by AD. The imaging of β-amyloid plaques by **13** in both murine and human tissue was confirmed by allocated red-fluorescent immunolabeling. It was shown for the first time that β-amyloid plaques can be successfully identified using a fluorescent, high-affinity AChE inhibitor. Two possible explanations can be given for this observation. Compound **13** might either bind to cholinesterases inside of the β-amyloid plaques, or to the amyloid structure itself. Based on the high affinity of **13** to AChE, we initially favored the former hypothesis. However, this explanation was ruled out by histochemical competition experiments with known cholinesterase inhibitors. Neither fasciculin-2, nor donepezil was capable of suppressing the staining by **13**. Nevertheless, separate experiments revealed the ability of **13** to inhibit AChE in several brain areas. It is therefore a unique feature of **13** that it detects β-amyloid plaques and inhibits tissue-bound AChE. The presence of three aromatic moieties in **13** may contribute to the high affinity to β-amyloid structures.[36,37]

Conclusions

The formation of β-amyloid plaques during the pathogenesis of AD is tightly linked to the presence of acetylcholinesterase. Staining methods for these plaques involve the use of antibodies or fluorescent dyes. We prepared a gorge-spanning, picomolar inhibitor of acetylcholinesterase carrying a fluorophore suitable for histochemical applications. The synthetic approach toward this inhibitor and its cholinesterase inhibiting properties are reported. Fluorescence characteristics and viability of this novel probe for histochemical identification of β-amyloid plaques in transgenic mice with β-amyloidosis or human fixed tissues from an AD case are presented. Switching from fixed tissues to *in vivo* experiments and further *in vitro* studies will be the subject of future investigations. In conclusion, **13** appears to be a valuable novel fluorescent probe for acetylcholinesterase and β-amyloid plaques.

Experimental

General methods and materials

Melting points were determined on a Boëtius melting-point apparatus, and are uncorrected. Compound **11** was prepared using the Büchi Glas Uster autoclave 'TinyClave'. Thin-layer chromatography was performed on Merck aluminum sheets, silica gel 60 F_{254}. Preparative column chromatography was performed on Merck silica gel 60, 70–230 mesh. ^{13}C NMR (125 MHz) and ^{1}H NMR spectra (500 MHz) were recorded on a Bruker Avance DRX 500 spectrometer; ^{13}C NMR signals were assigned on the basis of $^{13}C/^{1}H$ correlation experiments (HSQC and HMBC). Mass spectra were measured on a MS-50 A.E.I. (EI, 70 eV) and an API2000 (Applied Biosystems) spectrometer (ESI). Fluorescence spectra were obtained on a Perkin Elmer LS-55 spectrofluorimeter. Elemental analyses were performed with a Vario EL apparatus. Fluorescence labeling was analyzed with a confocal laser scanning microscope LSM 510 from Zeiss which was also equipped with a 405 nm diode and a 475 nm long pass filter. Histochemical documentation of AChE activity was performed with an Axiophot (Zeiss, Germany) equipped with an AxioCam HRC and the program AxioVision 3.1.2.1. Fasciculin-2 was purchased from Sigma (Steinheim, Germany), donepezil hydrochloride from Molekula (Dorset, UK). Recombinant hAChE and hBChE from human serum were obtained from Sigma (Steinheim, Germany), bovine serum albumin (BSA, fraction V) from AppliChem (Darmstadt, Germany). Rabbit antiserum directed against β-amyloid was obtained from Schering (Berlin, Germany), carbocyanine 3-conjugated goat-anti-rabbit antibodies from Dianova (Hamburg, Germany). Entellan was obtained from Merck (Darmstadt, Germany).

Preparation of 2-(4-(((7-(diethylamino)-2,4-dioxo-2*H*-chromen-3(4*H*)-ylidene)methyl)amino)phenyl)-*N*′-1,2,3,4-tetrahydroacridin-9-ylacetohydrazide (13)

To a solution of 7-(diethylamino)-4-hydroxy-2*H*-chromen-2-one (**5**; 2.0 mmol, 0.47 g) in refluxing glacial acetic acid (10 mL) 2-(4-aminophenyl)-*N*′-1,2,3,4-tetrahydroacridin-9-ylacetohydrazide (**12**; 2.0 mmol, 0.79 g) and triethyl orthoformate (4.0 mmol, 0.59 g) in glacial acetic acid (10 mL) was added dropwise over 5 min. The reaction mixture was refluxed for a further 5 min and stirred for 2 h. The solvent was evaporated *in vacuo*, the crude residue was suspended in water (100 mL) and the suspension was neutralized. A crude precipitate was filtered off and the aqueous phase was extracted with ethyl acetate (2 × 200 mL). The organic phases and a solution of the precipitate in ethanol were combined, dried using anhydrous sodium sulfate and evaporated *in vacuo*. The remaining residue was recrystallized from methanol/acetonitrile to obtain **13** (0.41 g, 35%) as a yellow precipitate, mpt 217 °C (decomposition). ^{1}H NMR (DMSO-d_6) δ 1.12 (t, 6 H, J = 6.9 Hz), 1.71–1.81 (m, 4 H), 2.76 (bs, 2 H), 2.88 (bs, 2 H), 3.43 (q, 4 H, J = 7.2 Hz), 3.47 (s, 2 H), 6.37 (app. s, 1 H), 6.66 (dd, 1 H, J = 1.9, 9.1 Hz), 7.29 (d, 2 H, J = 7.9 Hz), 7.30 (app. s, 1 H), 7.48 (d, 2 H, J = 8.5 Hz), 7.51 (app. t, 1 H, J = 7.7 Hz), 7.70 (app. s, 1 H), 7.71 (d, 1 H, J = 9.2 Hz), 7.77 (s, 1 H), 8.29 (d, 1 H, J = 7.6 Hz), 8.71 (d, 1 H, J = 10.7 Hz), 8.75 (app. bs, 0.5 H), 10.32 (s, 1 H), 13.47 (d, 0.5 H, J = 13.6 Hz); ^{13}C NMR (DMSO-d_6) δ 12.48, 22.47, 22.67, 24.93, 33.75, 39.53, 44.25, 96.56, 97.30, 108.04, 108.61, 115.85, 118.50, 119.13, 123.05, 123.60, 127.11, 127.99, 128.40, 130.62, 133.92, 136.92, 146.74, 148.51, 152.71, 153.48, 153.75, 156.76, 158.20, 163.14, 169.65, 179.67. EA found: C, 69.1; H, 6.2, N, 11.6. $C_{35}H_{35}N_5O_4 \cdot H_2O$ requires C, 69.2; H, 6.1, N, 11.5%. ESI-MS ($C_{35}H_{36}N_5O_4^+$) 590.3. For syntheses and elemental analyses of compounds **3**, **5**, **8**, and **10–12**, see S2 of the ESI†. For NMR spectra of compounds **3**, **5**, **8**, and **10–13**, see S10 of the ESI,† and for mass spectrometry analysis of **13**, see S17 of the ESI.†

Cholinesterase inhibition assay

Cholinesterase inhibition was assayed spectrophotometrically at 412 nm in duplicate experiments at six substrate (125, 250, 500, 750, 1000 and 1250 μM) and four to six inhibitor (AChE: 0, 250, 500, 750 pM; BChE: 0, 2 4, 6, 8, 10 nM) concentrations at 25 °C. Assay buffer was 100 mM sodium phosphate, 100 mM NaCl, pH 7.3. Stock solutions (~3 U mL^{-1}) of human acetyl- and butyrylcholinesterase in assay buffer were kept at 0 °C. Appropriate dilutions were prepared immediately before starting the measurement. Acetyl- or butyrylthiocholine (10 mM) and 5,5′-dithio-bis-(2-nitrobenzoic acid) (DTNB) (7 mM) were dissolved in assay buffer and kept at 0 °C. A stock solution of **13** was prepared in 10 mM hydrochloric acid and subsequently diluted in assay buffer. 50 μL of the DTNB solution, 10 μL of the inhibitor solution, and 10 μL of the cholinesterase solution were added to 870 μL of assay buffer and thoroughly mixed in a glass cuvette. After incubation for 15 min at 25 °C, the reaction was initiated by adding 50 μL of the substrate solution or appropriate dilutions and followed over 5 min. Kinetic analysis was performed using the software GraFit.[38] For Lineweaver–Burk analysis, see S5 of the ESI.†

Fluorescence measurements

Fluorescence spectra were obtained from a solution of **13** in methanol at a dilution suitable to meet the sensitivity level of the fluorimeter. The excitation wavelength was increased stepwise by 1 nm from 200 to 600 nm, while emission spectra were recorded in the same interval. To minimize the influence of diffuse scatter, control measurements were carried out using neat methanol. The emission spectra obtained from these control experiments were subtracted from those investigating **13** by a custom PERL script and the resulting data were analyzed using Gnuplot.[39] The scattered data obtained from the emission spectra was converted into a grid using the Gnuplot dgrid3d algorithm, where each data point is weighted with respect to its corresponding data point based on the Euclidian distance with a norm power of 4. The obtained grid was then analyzed with respect to excitation and emission maxima. The influence of protein binding on the fluorescence intensity of **13** was measured in assay buffer in the absence and presence of hAChE, hBChE and/or BSA at λ_{exc} = 405 nm and λ_{em} = 517 nm. A glass cuvette containing assay buffer (930 μL, 100 mM sodium phosphate, 100 mM NaCl, pH 7.3) was used to obtain blank recordings. A 3.66 μM solution (50 μL) of either hAChE, hBChE or BSA was added after 100 s and equilibrated for approximately 300 s while measuring fluorescence. Stock solutions of hAChE, hBChE and BSA were prepared according to their molecular weight and/or activity taken from vendor specifications. Subsequently, inhibitor solutions (20 μL of **13**, donepezil, or both; in assay buffer with 10% methanol) were added to obtain the following final concentrations, **13**: 20 nM (70 × IC_{50}), donepezil: 4 μM (700 × IC_{50}), methanol: 0.2%. Fluorescence recordings were continued for another 300 s. Linear parts were extracted from each section after visual inspection and subjected to standard statistical analysis (Grubbs' test, boxplot). For details, see S6 of the ESI.†

Histochemistry

A first series of histochemical experiments was performed with 30 μm-thick frozen sections from a paraformaldehyde-fixed autoptic tissue block containing the neocortical area 7 from a case with verified Alzheimer pathology. The tissue sample was used with permission and following the guidelines of the Local Ethical Committee in Leipzig, Germany. A second series of stainings was carried out with frontal sections containing the hippocampi from 12-month-old triple-transgenic mice carrying, as transgenes, mutated human β-amyloid precursor protein, presenilin-1 and τ.[20] These sections were made from brains perfused with 4% paraformaldehyde and 0.1% glutaraldehyde, post-fixed overnight with 4% paraformaldehyde, cryoprotected by equilibration with 30% sucrose and cut at 30 μm thickness using a freezing microtome. The use of animals in the present study was approved by the Animal Care and Use Committee of the University of Leipzig, Germany. All histochemical procedures were started by extensively rinsing of the 30 μm-thick free-floating sections with 0.1 M Tris-buffered saline (TBS), pH 7.4. The sections were then incubated with solutions containing 6.8 μM **13** in TBS for 90 min. After several rinses with TBS, non-specific binding sites for subsequently applied immunoreagents were blocked with 5% normal goat serum in TBS containing 0.3% Triton X-100.

The sections were then incubated with rabbit-anti-β-amyloid[40] (1 : 250 in the blocking solution) overnight. Following three washes with TBS, the tissue was processed with carbocyanine 3-conjugated goat-anti-rabbit IgG (20 μg mL^{-1} in TBS containing 2% BSA) for 1 h. In control experiments, the sections were incubated with the blocking solution without primary antibodies. Additionally, sections were first immunostained and then reacted with **13** as described above. Finally, all sections were washed with TBS and distilled water, mounted onto glass slides, air-dried and coverslipped with Entellan. The influence of fasciculin-2 and donepezil on the binding properties of **13** was investigated applying free-floating, 30 μm-thick tissue sections from 12–16-month-old triple transgenic mice, which had been prepared as described above. Sections were extensively rinsed with 0.1 M TBS, pH 7.4 and incubated with 3.1 μM ($130 \times IC_{50}$)[33] fasciculin-2 for 16 h or 145 μM ($25000 \times IC_{50}$)[28] donepezil for 90 min. Subsequently, the sections were incubated with 6.8 μM ($25000 \times IC_{50}$) **13** for 90 min, followed by Aβ-immunolabeling and tissue imaging as described above. In parallel, consecutive sections were processed in the same manner, but without fasciculin-2 or donepezil pretreatment. In addition, competition experiments were carried out as described above, where equipotent concentrations (145 μM donepezil, 6.8 μM **13**) or excess of donepezil (1450 μM donepezil, 6.8 μM **13**) were simultaneously used for incubation. For the labeling of senile plaques with **13** in the presence and absence of fasciculin-2, see S8 of the ESI.†

Histochemical enzyme activity assay

Two 15-month-old triple-transgenic mice and two 4-month-old wild-type mice were perfused with 4% paraformaldehyde without glutaraldehyde followed by post-fixation, cryoprotection and sectioning. After rinsing with TBS, 30 μm-thick free-floating frozen sections were incubated for 90 min with buffered solutions containing 68 μM, 6.8 μM, 680 nM, 68 nM and 0 nM **13**. Following three rinses with TBS, the sections were applied to AChE enzyme histochemistry with acetylthiocholine iodide as substrate at 37 °C according to the literature.[34] The development of insoluble brown reaction product was stopped after 30 or 90 min, respectively. Finally, the sections were washed with TBS, briefly rinsed with distilled water, mounted onto glass slides, air-dried and coverslipped with Entellan in toluene. For the histochemical enzyme activity assay with different concentrations of **13**, see S9 of the ESI.†

Acknowledgements

The authors thank Frank M. LaFerla and Salvatore Oddo (University of California, Irvine, USA) for triple-transgenic mice with age-dependent β-amyloidosis and τ pathology, and Thomas Arendt (University of Leipzig, Germany) for supplying the human brain sample. The excellent technical assistance of Ute Bauer, Renate Jendrek, Ulrich Gärtner and Stephanie Hautmann is gratefully acknowledged.

References

1 E. Giacobini and R. E. Becker, *J. Alzheimers Dis.*, 2007, **12**, 37.
2 C. E. Felder, S. A. Botti, S. Lifson, I. Silman and J. L. Sussman, *J. Mol. Graphics Modell.*, 1997, **15**, 318.
3 D. Muñoz-Torrero and P. Camps, *Curr. Med. Chem.*, 2006, **13**, 399.
4 D. J. Selkoe, *Physiol. Rev.*, 2001, **81**, 741.
5 T. Uchihara, *Acta Neuropathol.*, 2007, **113**, 483.
6 Z. X. Shen, *Med. Hypotheses*, 2004, **63**, 285.
7 M. A. Gerebtzhoff, *Cholinesterases: A histochemical contribution to the solution of some functional problems*, Pergamon Press, New York, 1959, pp 99–101.
8 M. J. Karnovsky and L. A. Roots, *J. Histochem. Cytochem.*, 1964, **12**, 219.
9 M. M. Mesulam and M. A. Morán, *Ann. Neurol.*, 1987, **22**, 223.
10 M. M. Mesulam, C. Geula and M. A. Morán, *Ann. Neurol.*, 1987, **22**, 683.
11 C. I. Wright, C. Geula and M. M. Mesulam, *Proc. Natl. Acad. Sci. U. S. A.*, 1993, **90**, 683.
12 N. C. Inestrosa and R. Alarcón, *J. Physiol. Paris*, 1998, **92**, 341.
13 C. Geula, B. D. Greenberg and M. M. Mesulam, *Brain Res.*, 1994, **644**, 327.
14 J. R. Saltmarsh, A. E. Boyd, O. P. Rodriguez, Z. Radić, P. Taylor and C. M. Thompson, *Bioorg. Med. Chem. Lett.*, 2000, **10**, 1523.
15 X. Huang, B. Lee, G. Johnson, J. Naleway, A. Guzikowski, W. Dai and Z. Darzynkiewicz, *Cell Cycle*, 2005, **4**, 140.
16 G. V. De Ferrari, W. D. Mallender, N. C. Inestrosa and T. L. Rosenberry, *J. Biol. Chem.*, 2001, **276**, 23282.
17 G. Amitai, Y. Ashani, A. Gafni and I. Silman, *Neurochem. Int.*, 1980, **2**, 199.
18 P. W. Elsinghorst, J. S. Cieslik, K. Mohr, C. Tränkle and M. Gütschow, *J. Med. Chem.*, 2007, **50**, 5685.
19 P. W. Elsinghorst, C. M. González Tanarro and M. Gütschow, *J. Med. Chem.*, 2006, **49**, 7540.
20 S. Oddo, A. Caccamo, J. D. Shepherd, M. P. Murphy, T. E. Golde, R. Kayed, R. Metherate, M. P. Mattson, Y. Akbari and F. M. LaFerla, *Neuron*, 2003, **39**, 409.
21 I. Schalk, L. Ehret-Sabatier, Y. Le Feuvre, S. Bon, J. Massoulie and M. Goeldner, *Mol. Pharmacol.*, 1995, **48**, 1063.
22 Y. P. Auberson, Patent WO2003074519. *Chem. Abstr.* 2003, **139**, 245901.
23 R. L. Atkins and D. E. Bliss, *J. Org. Chem.*, 1978, **43**, 1975.
24 A. Knierzinger and O. S. Wolfbeis, *J. Heterocycl. Chem.*, 1980, **17**, 225.
25 A. Musiał, M. Bajdal and B. Malawska, *Curr. Med. Chem.*, 2007, **14**, 2654.
26 M. L. Bolognesi, A. Minarini, M. Rosini, V. Tumiatti and C. Melichiorre, *Mini-Rev. Med. Chem.*, 2008, **8**, 960.
27 D. Muñoz-Torrero, *Curr. Med. Chem.*, 2008, **15**, 2433.
28 H. Sugimoto, Y. Iimura, Y. Yamanishi and K. Yamatsu, *J. Med. Chem.*, 1995, **38**, 4821.
29 G. V. De Ferrari, M. A. Canales, I. Shin, L. M. Weiner, I. Silman and N. C. Inestrosa, *Biochemistry*, 2001, **40**, 10447.
30 N. C. Inestrosa, M. C. Dinamarca and A. Alvarez, *FEBS J.*, 2008, **275**, 625.
31 Y. Mimori, S. Nakamura and M. Yukawa, *Behav. Brain Res.*, 1997, **83**, 25.
32 Y. Bourne, Z. Radić, G. Sulzenbacher, E. Kim, P. Taylor and P. Marchot, *J. Biol. Chem.*, 2006, **281**, 29256.
33 B. Lockhart, M. Closier, K. Howard, C. Steward and P. Lestage, *Naunyn-Schmiedeberg's Arch. Pharmacol.*, 2001, **363**, 429.
34 J. Andrä and Z. Lojda, *Histochemistry*, 1986, **84**, 575.
35 Y.-P. Pang, P. Quiram, T. Jelacic, F. Hong and S. Brimijoin, *J. Biol. Chem.*, 1996, **271**, 23646.
36 A. Lockhart, L. Ye, D. B. Judd, A. T. Merritt, P. N. Lowe, J. L. Morgenstern, G. Hong, A. D. Gee and J. Brown, *J. Biol. Chem.*, 2004, **280**, 7677.
37 A. A. Reinke and J. E. Gestwicki, *Chem. Biol. Drug Des.*, 2007, **70**, 206.
38 R. J. Leatherbarrow, *GraFit Version 5.13*, Erithacus Software Ltd.Horley, UK, 2007.
39 Gnuplot Version 4.2, http://www.gnuplot.info (January 22, 2009).
40 T. Siegemund, B. R. Paulke, H. Schmiedel, N. Bordag, A. Hoffmann, T. Harkany, H. Tanila, J. Kacza and W. Härtig, *Int. J. Dev. Neurosci.*, 2006, **24**, 195.

